Pakistan Veterinary Journal

ISSN: 0253-8318 (PRINT), 2074-7764 (ONLINE)
DOI: 10.29261/pakvetj/2026.066

RESEARCH ARTICLE

CRISPR-Cas9 revealed that the *Nlrp3*-2906G Allele Impairs Phagocytosis of Porcine Alveolar Macrophages to Enhance *Mycoplasma hyopneumoniae* Susceptibility in Pigs

Lingxi Zhang[1], Zengcan Wang[1], Zhiyi Zhang[1], Gang Zhao[1], Siyang Zhang[2], Jine Yu[2], Mei Liu[3], Xiaoming Huang[1], Chong Yin[1], Shifeng Hu[1] and Guiping Wang[1*]

[1]College of Veterinary Medicine, Hunan Agricultural University, Changsha 410128, Hunan, China; [2]Hunan Liushahe Spotted Pig Ecological Animal Husbandry Co., Ltd. Changsha 410600, Hunan, China; [3]College of Animal Science and Technology, Hunan Agricultural University, Changsha 410128, Hunan, China
*Corresponding author: wanggp003@hunau.edu.cn

ARTICLE HISTORY (25-738)

Received: July 27, 2025
Revised: March 10, 2026
Accepted: March 11, 2026
Published online: March 15, 2026

Key words:
Mycoplasma hyopneumoniae
Ningxiang Pig
NLRP3
Porcine Alveolar Macrophages

A B S T R A C T

Chinese indigenous pig breeds are generally more susceptible to *Mycoplasma hyopneumoniae* (Mhp), however, the underlying molecular mechanisms remain poorly understood. At slaughter, Ningxiang pigs (n=77) exhibited a 2.6-fold higher Mhp detection rate and a 1.5-fold higher average Goodwin (GW) score than Duroc×Landrace×Yorkshire (DLY) pigs (n=83), (P<0.01). Here, we demonstrated that genetic variation at position 2906 of the *NOD-like receptor family pyrin domain containing 3* (*Nlrp3*) gene in Ningxiang pigs (as compared to DLY pigs) was associated with reduced phagocytic efficiency of Porcine Alveolar Macrophages (PAMs) against Mhp, primarily by suppressing the expression of *Nlrp3* and *interleukin-1β* (*Il-1β*), thereby compromising host immune defense and enhancing susceptibility to Mhp infection in Ningxiang pigs. Genetic sequencing revealed that all PAMs derived from Ningxiang pigs harbored a Guanine (G) allele at position 2906 of the *Nlrp3* gene, whereas 88.64% of DLY pig-derived PAMs carried an Adenine (A) allele at this locus. Site-directed mutagenesis of *Nlrp3*-2906G PAMs to *Nlrp3*-2906A PAMs by CRISPR-Cas9 was performed to investigate the functional consequences. Transcriptomic analysis revealed that the p.Q969 (A allele) mutation significantly upregulates *Nlrp3* mRNA expression. Transcriptomic analysis and ELISA validated that this improvement was mediated by upregulated expression of *Nlrp3* and *Il-1β*. Furthermore, functional assays demonstrated that the A allele enhanced phagocytic efficiency against pathogens by an average of 1.8- to 3.8-fold (P<0.01). Mhp Real-time fluorescence quantitative PCR (qPCR) and fluorescence tracing assays demonstrated the phagocytic efficiency of PAMs derived from Ningxiang pigs against Mhp was approximately 2.65-fold lower than that in DLY pigs (P<0.01), indicating a significant impairment in Mhp clearance. Collectively, these results suggest that the *Nlrp3*-2906G variant enhances Mhp susceptibility in Ningxiang pigs by impairing PAM-mediated microbial clearance, revealing a novel genetic mechanism that sheds light on the specific susceptibility of pigs to Mhp.

To Cite This Article: Zhang L, Wang Z, Zhang Z, Zhao G, Zhang S, Yu J, Liu M, Huang X, Yin C, Hu S and Wang G, 2026. CRISPR-Cas9 revealed that the *Nlrp3*-2906G allele impairs phagocytosis of porcine alveolar macrophages to enhance *Mycoplasma hyopneumoniae* susceptibility in pigs. Pak Vet J, 46(4): 940-951. http://dx.doi.org/10.29261/pakvetj/2026.066

INTRODUCTION

Mycoplasma hyopneumoniae is the causative agent of porcine epidemic pneumonia, a chronic respiratory disease affecting pigs of all age groups. Susceptibility to Mhp infection varies widely among pig breeds (Shao, 2003; Sousa *et al*., 2024). It is noteworthy that the local Chinese breed, Jiangquhai pig, has a higher prevalence of Mhp infection and more severe lung lesions compared to imported breeds (Maingi *et al*., 2014; Ni *et al*., 2019). After artificial inoculation with Mhp, different breeds showed different immune response profiles. For example, Meishan pigs (another native Chinese breed) exhibit a more severe clinical phenotype of Mhp (Fang *et al*., 2015). These observations suggest a potential imbalance in the innate immune response of Chinese native pig breeds. Specifically, after infection with Mhp, their immune systems may become dysfunctional, triggering an

exacerbated inflammatory response and subsequent tissue damage. Ningxiang pigs are a well-known local pig breed in China and a core germplasm resource in Hunan. They are valued for their excellent meat quality and high intramuscular fat content (Yin *et al*., 2023; Li *et al*., 2025). Anecdotal evidence suggests that during the fattening stage, clinical signs of Mhp infection in Ningxiang pigs are reported to be more severe than in common pigs, and Mhp-induced lung lesions are more pronounced at slaughter. However, these observations require rigorous scientific validation to establish their reliability and potential mechanisms.

Mhp-induced lung lesions were more severe in Ningxiang pigs, suggesting that specific cellular components of their lungs may be more vulnerable during Mhp infection. PAMs are the first line of innate immune defense of the pig lung. They parasitize the alveolar surface and fight respiratory pathogens through phagocytosis (Mei *et al*., 2023; Zhou *et al*., 2025). During the early stages of Mhp infection and colonization, direct interaction with resident PAMs in the lungs is inevitable (Lai *et al*., 2023), which may facilitate persistent pulmonary colonization (Deeney *et al*., 2019; Wen *et al*., 2022) and long-term survival of Mhp in porcine lung tissue (Zhou, 2021). We therefore hypothesize that compared to DLY pigs, PAMs derived from Ningxiang pigs exhibit less efficient phagocytic activity, thereby enabling easier establishment of Mhp in the lungs.

If PAMs derived from Ningxiang pigs exhibit inefficient phagocytosis of Mhp, the underlying molecular mechanisms remain unclear. Mhp adsorption to PAMs surfaces triggers the TLR2/6 heterodimer. This activates the NF-κB pathway and transmits signals to the NLRP3 inflammasome (Muneta *et al*., 2003). The NLRP3 inflammasome is a multi-protein complex comprising the sensor protein NLRP3, apoptosis-associated speckle-like protein (ASC), and effector caspase-1 (Xia *et al*., 2023). Beyond its canonical role in inflammasome assembly and IL-1 β maturation, NLRP3 also regulates non-canonical functions. These include phagosomal maturation and microbicidal activity. Polymorphisms in the *Nlrp3* gene may thus influence not only inflammatory responses but also fundamental phagocytic processes (Kagan JC *et al.*, 2013; Guo S *et al.*, 2015). Emerging evidence highlights the critical regulatory role of the NLRP3 inflammasome in Mhp infection (Zhang *et al*., 2023). Notably, the amino acid at position 969 of NLRP3 (encoded by nucleotide at position 2906) exhibits high polymorphism, with single-nucleotide polymorphisms (SNP) at position 2906 widely distributed in commercial pig breeds such as Landrace, Large White, and Berkshire pigs (Tohno *et al*., 2016). Clinical population surveys and statistical analyses have shown that amino acid polymorphisms at the NLRP3-969 locus are associated with IL-1β secretion levels and GW scores (Shinkai *et al*., 2018; Suzuki *et al*., 2022). Therefore, we hypothesized that *Nlrp3*-2906 site polymorphisms are present in PAMs of both DLY and Ningxiang pigs and that these variants are associated with differences in PAMs phagocytic efficiency.

On the basis of the above genetic determinants of Mhp susceptibility in pig breeds, this study used Ningxiang and DLY pigs as research models to investigate the relationship between SNP distribution at the 2906 locus of the *Nlrp3* gene and Mhp susceptibility and its potential molecular mechanisms. The aim of this study was to reveal the genetic basis of breed-specific disease resistance phenotypes by analyzing the genomic variation at this locus, thus providing a theoretical framework for the development of breeding strategies for Mhp- resistant pigs.

MATERIALS AND METHODS

Ethical Statement: This study was approved by the Biomedical Research Ethics Committee of Hunan Agricultural University (Approval No. 2024-140) and was conducted in accordance with ARRIVE guidelines and national animal welfare regulations.

Experimental animals: A total of 77 Ningxiang pigs and 83 DLY pigs were collected as tissue samples at a slaughterhouse. In addition, 102 newborn piglets (0 days old) were selected, including 54 Ningxiang pigs with an average weight of 0.50kg and 48 DLY pigs with an average weight of 0.65kg. The two breeds had a comparable gender ratio. All Ningxiang pigs were sourced from Liushahe Huazhu Ecological Animal Husbandry Co., Ltd. in Hunan Province, China, while all DLY pigs were obtained from Hunan New Five Elements Livestock Co., Ltd. in China.

Cell lines: PAMs were isolated from neonatal piglets (Wang, 2015) by lung lavage with ice-cold sterile PBS containing penicillin/streptomycin. The lavage fluid was centrifuged (800 ×g, 10min, 4°C), and the cell pellet was washed three times with PBS before being resuspended in complete RPMI-1640 medium supplemented with 10% FBS. After a 2-hour adherence period at 37°C in a 5% CO_2 incubator, non-adherent cells were removed. The resulting adherent PAMs were used for subsequent experiments. The PAM cell line 3D4/21 was purchased from Cyagen Biosciences (Suzhou, China). 3D4/21 was cultured in RPMI-1640 medium (10% FBS, 1% penicillin-streptomycin) at 37°C with 5% CO_2. Cells at passages 3-6 were used for all experiments.

Bacterial and virus Strains： Mhp strain YY was kindly provided by Huazhong Agricultural University (Wuhan, China).*Streptococcus suis* strain DY and *Porcine Reproductive and Respiratory Syndrome Virus* (PRRSV) strain JXA1 were supplied by Hunan Agricultural University (Changsha, China).

Mhp culture: Mhp was cultured in a liquid medium (Wang, 2015). The base solution, containing PPLO broth, BHI, yeast extract, glucose, lactalbumin hydrolysate, sodium pyruvate, and phenol red in 400 mL ultrapure water, was autoclaved (115°C, 10 min). After cooling, horse serum, mycoplasma-negative swine serum, Hank's Balanced Salt Solution, and penicillin (0.1mg/mL final) were added, and the pH was adjusted to 7.4–7.6. Cultures were inoculated at 10% and incubated statically at 37°C for 3–5 days, with harvest occurring at medium color change (yellow).

DNA sequencing analysis: Genomic DNA was extracted from the samples using a commercial kit (HunanGuanmu, China, Cat. No.: EX18250201). Specific primers for Mhp (Wang, 2015) and *Nlrp3* (Suzuki *et al*., 2022) (Table 1)

were synthesized. PCR amplification was performed as follows: initial denaturation at 98°C for 5min; 35/33 cycles of denaturation at 94/95°C for 30s, annealing at 60/55°C for 30s, and extension at 72°C for 50s/1min; followed by a final extension at 72°C for 5min. The PCR products were analyzed by 1% agarose gel electrophoresis. Target bands were excised and sent for sequencing to Sangon Biotechnology (Shanghai, China).

Table 1: List of primers used in this study.

Target	Sequences 5' to 3'
Mhp-F	GAGCCTTCAAGCTTCACCAAGA
Mhp-R	TGTGTTAGTGACTTTTGCCACC
Nlrp3-F	CCAAGCTTGTTAATCTTGTGC
Nlrp3-R	AAGTGCAAATGAAGCCATCC
gRNA	TGCCTAGGCTCAGCTTTCGC-AGG
Oligo	GAGAACTGCAGCCTCACATCACACTGCTGCTGGGAT
	CTTTCCACACTTCTGACTTCTAACCAGAGCCTGCGAA
	AACTGAGCCTAGGCAACAATGACCTGGGTGATCTGG
	GGGTCATGCTACTCTGTGAAGTGTTG

qPCR: Quantification of Mhp or PRRSV phagocytosed (including attachment and internalization) by PAMs using qPCR. Following co-incubation, PAMs were harvested and subjected to co- extraction of DNA/RNA using a commercial nucleic acid extraction kit (Hunan Guanmu, China, Cat. No.: EX18250201). The phagocytosed bacterial/viral load was then quantified with species-specific qPCR assays targeting Mhp or PRRSV respectively, performed according to the manufacturers' protocols.

Enzyme-linked immunosorbent assay (ELISA): The concentration of Porcine IL-1β in cell culture supernatants following co-incubation of PAM with Mhp was measured according to the instructions of the porcine IL-1β ELISA research kit (JingMei Biotechnology, China, Cat. No.: JM-01256P1).

Fluorescence tracing assay: The experiment was divided into two groups: the Mhp- PAM^{Q} (Q: Gln, coded by 2906A) interaction group and the Mhp- PAM^{R} (R: Arg, coded by 2906G) interaction group，with three biological replicates per group. Both groups were subjected to the same experimental procedures. DiD Perchlorate stock (BioLab Scientific, Cat. No.:SY0585) solution (5mM) was prepared by dissolving DMSO per manufacturer's instructions and stored at -20°C. Working dilutions (1:1000) were prepared fresh. Mhp cells were pelleted (10,000 r/min, 15min), resuspended in DiD working solution, and incubated overnight (37°C, 5% CO_2, dark). Excess dye was removed via three PBS washes. The stained Mhp was resuspended in RPMI-1640 medium supplemented with 2% fetal bovine serum.Poly-L-lysine-treated 96-well plates (Biosharp, China) were used for co-incubation of PAM with DiD-labeled Mhp (MOI 10) at 3, 6, and 12h. Cells were fixed (4% PFA, 10min), permeabilized (0.2% Triton X-100, 20min), and blocked (1% BSA, 30min). β-actin antibody (1:200) (Proteintech,China, Cat. No.:CL488-66009) was applied overnight (4°C, dark), followed by DAPI staining (5min, dark). After three PBS washes, samples were imaged via inverted fluorescence microscopy. Data are presented as the mean fluorescence intensity (MFI) from three independent experiments, with each condition performed in triplicate.

***Nlrp3* gene mutation：** Genomic DNA was extracted from PAMs 3D4/21 per kit instructions according to the manufacturer's instructions. A pair of specific primers (forward: 5'-TGGAGAGGTAAATACTGGTGTTGC-3'; reverse: 5'-GTTTTCACTGGGACTTGTGTTTCT-3') was designed and synthesized to amplify the genomic region encompassing the gRNA target site. PCR was run with this profile: 94°C for 3 min; 35 cycles of (94°C for 30s, 62°C for 35s, 65°C for 50s); and 65°C for 10min. PCR products were electrophoresed on 1% agarose gel; target bands were excised (TINGEN®, Cat. No.: DP209) and subjected to sequencing.

Following this, RNP electroporation was performed: 1 μL of 0.2 nmol Cas9 protein, 1μL of 0.1 nmol gRNA, and 1μL of 0.5nmol oligo (Table 1) were co-incubated to form ribonucleoprotein complexes. After preparing the electroporator and collecting the cells, the cell suspension was transferred into an electroporation cuvette and subjected to electroporation at 520V. The electroporated cells were then inoculated into culture medium and mixed thoroughly.

For cell pool analysis, genomic DNA from PAMs 3D4/21was extracted per kit protocol (Simgen, Cat. No.:3002250). The target site was amplified and sequenced. Mixed-cell sequences were analyzed via Tide (https://tide.nki.nl/) and Synthego ICE (https://ice.synthego.com/) against wild-type controls. Based on the results, cell populations exhibiting higher HDR efficiency were selected for single-cell plating to isolate clones with the desired edit. Monoclonal cell lines were subsequently established via limiting dilution cloning. Single clones were expanded to 60% confluency in 96-well plates, then subcultured into replicate plates. Genomic DNA from monoclonal cells underwent Sanger sequencing of target loci.

Transcriptome sequencing: PAM^{Q} and PAM^{R} cells were infected with Mhp at a MOI of 10 and co-incubated for 24 hours. Each treatment group consisted of three independent biological replicates (n = 3). Total RNA was extracted using TRIzol™ reagent. RNA sequencing libraries were constructed and sequenced on an Illumina platform to generate raw data.

Information was statistically analyzed, and FastQC was used for visual assessment of the sequencing data quality of samples. The raw sequencing data contained adapter-ligated and low-quality sequences. To ensure the quality of bioinformatics analysis, Fastp (Chen *et al*., 2018) was used for data processing: filtering the raw data to obtain clean data.

Following data quality control, the quality-controlled sequencing reads were subjected to reference sequence alignment. Quality-controlled sequencing reads were aligned to the reference genome (Sus scrofa Sscrofa11.1) using HISAT2 (Kim *et al*., 2015). Alignment metrics including mapping rate, insert size distribution, and strand specificity were quantified with RSeQC (Wang *et al*., 2012). Differential alternative splicing events were detected using rMATS (Shen *et al*., 2014). Transcriptome assemblies were generated from aligned BAM files using StringTie (Pertea *et al*., 2015). Novel transcribed regions were identified by comparing assemblies against annotated gene models via GffCompare.

To facilitate cross-sample comparisons, gene-level expression was calculated as TPM (Transcripts Per Million)

using FeatureCounts. This unit quantifies the relative abundance of a transcript in the total RNA pool and serves as a common method for estimating expression levels because it normalizes for the effects of sequencing depth, gene length, and sample-specific distribution of reads.

$$TPM_i = \frac{X_i}{L_i} * \frac{1}{\sum_j \frac{X_j}{L_j}} * 10^6$$

$$X_i = total\ exon\ fragment/reads \quad L_i = \frac{exon\ length}{KB}$$

We performed differential gene expression analysis using DESeq2 with criteria of qValue < 0.05 and |log2FoldChange| > 1.0 to identify significant DEGs. These DEGs were mapped to STRING for PPI network construction. Venn diagrams, heatmaps, and cluster analyses were generated based on differential results.

Hypergeometric distribution-based gene enrichment analysis was performed using clusterProfiler to identify functional categories enriched with DEGs (corrected P-value/Qvalue<0.05). GO, KEGG, and GSEA (Subramanian *et al*., 2005) were conducted via topGO, clusterProfiler, and GSEA, respectively.

Statistical analysis: All values are expressed as means ± SDs from at least three independent experiments. Statistical significance was determined by Student's t-test when only two groups were compared or by one-way analysis of variance (ANOVA) when more than two groups were compared. Statistical analyses were performed using GraphPad Prism 9.5 (GraphPad Software, San Diego, CA, USA). ****P<0.0001, ***P<0.001, **P<0.01, *P<0.05 were considered to be statistically significant at different levels.

RESULTS

Comparison of pathological damage and Mhp positive rate between Ningxiang pigs and DLY pigs: It was collected that lung tissues from Ningxiang pigs and DLY pigs at a slaughterhouse to assess interspecific differences in the degree of pathological damage in lung tissues and the positive rate of Mhp. Pigs infected with Mhp exhibited flesh-like lung lesions, consistent with descriptions in the literature (Ferreira *et al*., 2021). Notably, the severity of lung lesions was significantly higher in Ningxiang pigs than in DLY pigs (Fig.1A). The pathological damage in porcine lung tissues was quantitatively evaluated using the GW score (Fig.1B). The results demonstrated that the average pathological score of Ningxiang pigs (27.416) was significantly (P<0.01) higher than that of DLY pigs (18.229) (Fig.1C). PCR detection (Fig.1D) revealed that the Mhp positive rate in Ningxiang pigs (64.94%) was significantly higher than that in DLY pigs (25.30%) (Fig.1E). Collectively, these results indicate that Ningxiang pigs display higher susceptibility to Mhp infection compared to DLY pigs.

Differences in Phagocytic efficiency of PAMs between Ningxiang pigs and DLY pigs: To investigate the correlation of phagocytic efficiency of PAMs between Ningxiang pigs and DLY pigs, 102 PAMs were isolated and purified from newborn piglets (54 Ningxiang pigs and 48 DLY pigs) according to the method described by Wang (2024). To assess the phagocytic efficiency of each PAM from 102 independent primary cell cultures, cells were individually co-incubated with Mhp (MOI = 10) for 2.5 hours, the nucleic acid copy number of phagocytosed Mhp was then quantified by qPCR，and phagocytic efficiency was calculated using the following formula:Phagocytic efficiency (%) = $2^{(\text{Ct of input Mhp} - \text{Ct of Mhp in PAMs at 2.5 h})} \times 100\%$. Results showed that the phagocytized efficiency of Mhp in PAMs from Ningxiang pigs (5.82%) was significantly lower than that from DLY pigs (15.42%) (P<0.0001) (Fig.2A, B). This indicates that PAMs from Ningxiang pigs exhibit significantly weaker phagocytic efficiency toward Mhp compared to those from DLY pigs. Drawing on Suzuki (2022) study on variations in pulmonary lesion scores (GW scores) across pig farms and Duan (2020) research on NLRP3 inflammasome p. Leu 969 Pro polymorphism, we hypothesize that the interbreed difference in PAM phagocytosis efficiency may be associated with SNPs at the *Nlrp3* gene locus (Keel *et al*., 2018).

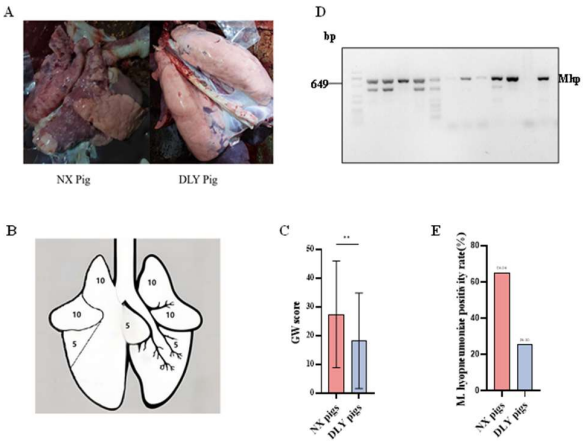

Fig.1: Lung pathological injury and Mhp positive rate in Ningxiang pigs and DLY pigs. (A) Gross Pathological changes in lungs from Ningxiang pig (left) and DLY pig (right). (B)Representative GW (55-point) score for mycoplasma pneumonia-like lesions in pigs. (C) GW score was used to evaluate the degree of pathological injury of lung tissues in 77 Ningxiang pigs and 83 DLY pigs, with a mean GW score of 27.416 for Ningxiang pigs and 18.229 for DLY pigs. (D) Mhp-PCR agarose gel electrophoresis of porcine lungs. (E) The positive rate of Mhp-PCR in 77 Ningxiang pigs and 83 DLY pigs showed that the Mhp-positive rate was 64.94% in Ningxiang pigs and 25.30% in DLY pigs. Statistical significance: ***P<0.0001, ***P <0.001, **P<0.01, *P<0.05.

***Nlrp3* c.2906A>G Polymorphism Detection and Its Correlation with PAM Phagocytic Activity:s** Using the gene sequencing approach described by Yuan (2021), we successfully identified SNPs at locus 2906 of the *Nlrp3* gene in 39 Ningxiang pigs and 44 DLY pigs. Sequencing revealed a SNP at codon c.2906, corresponding to amino acid position 969 of the NLRP3 protein (Fig.2C). All Ningxiang pigs (39/39) carried a G base (encoding arginine, R) at locus 2906, whereas 88.64% (39/44) of DLY pigs carried a A base (encoding glutamine, Q) at this locus, with the remaining 5 individuals harboring the G base (Fig.2D). The difference in genotype

distribution among hybrids was statistically significant (Gilroy *et al*., 2022). Functional correlation analysis showed that PAMs carrying the c.2906G allele phagocytosed Mhp significantly less efficiently than those carrying the c.2906 A allele (P<0.001) (Fig.2E). Specifically, the phagocytic efficiency at 2.5 h was 7.28% in PAMs with the c.2906G allele, compared with 15.01% in those harboring the c.2906A allele. These findings indicated that PAMs from Ningxiang pigs have weaker phagocytic activity for Mhp compared with PAMs from DLY pigs. Collectively, these data suggest that the c.2906 A>G polymorphism in the *Nlrp3* gene is associated with breed-specific differences in Mhp infection resistance and correlates with variations in PAMs phagocytic capacity. To directly validate the causal relationship between the *Nlrp3* c.2906 A>G polymorphism and PAMs phagocytic efficiency, we employed CRISPR- Cas9 gene editing technology to introduce site- specific modifications in a cellular model, aiming to elucidate how mutations at this locus affect PAM- mediated phagocytosis of Mhp.

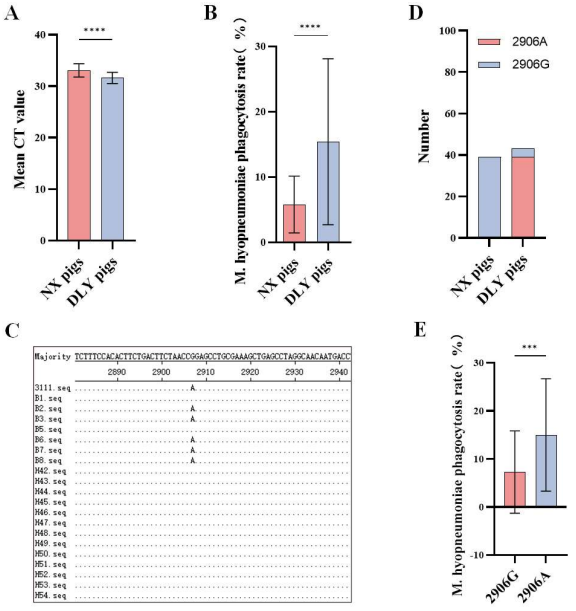

Fig.2: Phagocytic efficiency against Mhp and *Nlrp3* c.2906A>G genotypes in PAMs from Ningxiang pigs and DLY pigs. (A) Quantification of phagocytosed Mhp in PAMs from Ningxiang pigs (average Ct 33.07) and DLY pigs (average Ct 31.60) by qPCR.(B) Phagocytic rates in Mhp by PAMs derived from Ningxiang pigs (average 5.82%) and DLY pigs (average 15.42%) based on the Ct values of qPCR. (C) SNPs at 2906 loci were detected in 83 samples using MegAlign software. (D)Genotype dstribution of the *Nlrp3* c.2906A>G polymorphism in Ningxiang pigs and DLY pigs. All Ningxiang pigs (39/39) were homozygous for the G allele, while 88.64% (39/44) of DLY pigs carried the A allele at this locus. (E) Correlation between Nlrp3 c.2906A>G genotype and Mhp phagocytic efficiency in PAMs. AMs carrying the c.2906G allele exhibited a significantly lower Mhp phagocytic efficiency (7.28%), compared with 15.01% in PAMs carrying the c.2906A allele. Statistical significance: ****P<0.0001, ***P<0.001, **P<0.01, *P< 0.05.

***Nlrp3* c.2906A>G mutation mediated phagocytic efficiency of PAMs:** It was used for electroporation-mediated CRISPR- Cas9 gene editing technology (Janik *et al*., 2020) to introduce a point mutation in the *Sus scrofa Nlrp3* gene within PAM 3D4/21 (PAM^R) cells: Exon 10 p.R969Q (CGG → CAG; c. 2906G >A). This edit also includes a synonymous mutation, p. K973= (AAG→AAA) (Fig.3A). Following electroporation, we selected the cell pool with the highest HDR efficiency (57% as analyzed by Synthego, 26.2% as determined by TIDE) for monoclonal cell line isolation. The monoclonal cell lines were isolated and validated via PCR and Sanger sequencing (Fig.3B, C). We successfully generated homozygous *Sus scrofa* NLRP3 (p.R969Q)-mutant cells (PAM^Q) (Fig.3D). To investigate the correlation between the NLRP3 p.R969Q mutation and pathogenic microorganism clearance efficiency, we first compared the ability of PAM^Q (mutant) cells and PAM^R (wild-type) cells to phagocytose Mhp. Both PAM^Q cells and PAM^R cells were co-incubated with Mhp (MOI = 10) for 3, 6, and 12 hours, respectively. The efficiency of Mhp phagocytosis by PAMs was quantified using both qPCR and fluorescence tracing assays (Zhou, 2021), and phagocytic efficiency was calculated using the following formula: Phagocytic efficiency (%) = 2(Ct of input Mhp − Ct of Mhp in PAMs at 2.5 h)×100%.Results showed that PAM^Q cells exhibited 2.30-, 1.81-, and 2.01-fold higher phagocytic efficiency at 3, 6, and 12 h of incubation, compared with PAM^R cells, respectively (Fig.4A, B). The average fluorescence intensity and total fluorescence density exhibited consistent trends, with PAM^Q showing approximately 2.68-, 1.25-, and 1.63-fold higher signals than PAM^R at 3, 6, and 12 h, respectively (Fig.4C, D). It showed significantly higher Mhp uptake (P<0.01) in PAM^Q cell compared to PAM^R cells (Fig.4E). Next, we assessed the effect of the mutation on phagocytosis of other pathogens. Phagocytosed bacterial load was measured using colony forming unit (CFU) counts after 3, 6 and 12h of co-incubation with *streptococci* (MOI = 10), according to the method described by Arora et al. (2023). The phagocytic efficiency of PAM^Q was 3.22-, 2.73-, and 2.60-fold higher than that of PAM^R at 3, 6, and 12 h post-incubation, respectively (Fig.4F). The NLRP3 p.R969Q mutation significantly (P<0.0001) enhanced the phagocytosis of *streptococci* by PAMs. To investigate the effect of the NLRP3 p.R969Q mutation on different stages of PRRSV infection, intracellular viral RNA levels were quantified at multiple time points using qPCR. At 3 h post-infection, the Ct value of PAM^Q was undetectable (0), whereas that of PAM^R was 37.58. At 6 h post-infection, the Ct value of PAM^Q was 1.01-fold that of PAM^R, while at 12 h post-infection, the Ct value of PAM^R was 1.06-fold that of PAM^Q (Fig.4G). The mutation significantly reduced viral RNA levels at 3 and 6h post-infection (P<0.05), indicating impaired viral internalization. In contrast, viral RNA levels were significantly enhanced at 12 h post-infection (P<0.0001), suggesting facilitated viral replication. These findings suggest that while the NLRP3 p.R969Q mutation enhances phagocytic clearance by Mhp and *Streptococcus suis*, it has a stage-specific effect on PRRSV infection, inhibiting early internalization while promoting subsequent replication.

NLRP3 p.R969Q mutation enhanced IL-1β secretion: Bioinformatics analysis revealed that residue 969 of the NLRP3 protein is located in the coding region of the NLRP3 leucine-rich repeat (LRR) sequence structural domain (Fig.5A, B). Upon Mhp stimulation, the LRR structural domain of NLRP3 becomes activated and recruits caspase-1 by the adaptor protein ASC. This cascade subsequently triggers the activation of IL-1β, initiates inflammatory responses, and regulates the phagocytic efficiency of peripheral PAMs (El-Sharkawy *et al*., 2020).

To explore the time-dependent effect of this mutation on IL-1β secretion, PAM^{Q} cells and PAM^{R} cells were stimulated with Mhp (MOI=10), respectively, and IL-1β levels in cell culture supernatants were measured at 3, 6 and 12 h.post-stimulation by ELISA. The differences in IL-1β secretion between PAM^{Q} and PAM^{R} were 5.39, 2.30, and 8.65 pg/mL at 3, 6, and 12 h post-stimulation, respectively (Fig.5C), all indicating that PAM^{Q} secreted more IL-1β than PAM^{R}.To explore the dose-dependent effect of Mhp stimulation on inflammatory cytokine production, IL-1β secretion in the supernatants of PAM^{Q} and PAM^{R} cells was detected by ELISA after treatment with Mhp at MOIs of 1, 3, and 10 for 12 h by ELISA. At 12 h post-stimulation, the corresponding differences were −3.713, 3.65, and 8.653 pg/mL at MOIs of 1, 3, and 10, respectively (Fig.5D), PAM^{Q} secreted less IL-1β than PAM^{R} at MOI 1, but more at MOIs 3 and 10.

Transcriptome analysis: Following co-incubation of Mhp with PAM^{Q} and PAM^{R}, respectively, transcriptome sequencing was performed. To ensure data quality, raw data underwent quality control in this study, and differentially expressed genes (DEGs) in the transcriptome were identified macroscopically. It presented the VENN diagram comparing the two groups (Fig.6A). Specifically, 16893 genes were shared between the two groups, with 1044 and 980 genes unique to the PAM^{R} and PAM^{Q} groups, respectively. Results showed that a total of 1,340 DEGs were identified between the two groups, with 867 genes significantly upregulated and 473 genes significantly downregulated (Fig.6B, C). The PCA plot demonstrated clear differences between the two groups based on gene expression levels (Fig.6D). The GO database is categorized into three main ontologies: molecular function (MF), cellular component (CC), and biological process (BP) (Fig.6E). GO annotation statistics showed that the CC, BP, and MF categories contained 17,525, 16,309, and 15,110 annotated Unigenes in the GO database, respectively. Concurrently, the KEGG annotation bar plot showed that DEGs were enriched in the regulation of carbohydrate and lipid metabolism, cell growth and death, and the immune system (Fig.6F). DEGs between the two groups were also involved in GO terms such as cell surface receptor signaling pathway, extracellular vesicle, and igand-gated monoatomic cation channel activity (Fig.6G). Additionally, the PI3K/AKT signaling pathway, Cytokine-cytokine receptor interaction, Arachidonic acid metabolism, and Hippo signaling pathway were enriched in KEGG enrichment analysis (Fig.6H).

The KEGG pathway analysis showed that the mRNA expression level of the *Nlrp3* gene in PAM^{Q} was 3.88 - fold higher than that in PAM^{R}. The *Nlrp3* gene is mainly involved in the Necroptosis signaling pathway, the NOD - like receptor signaling pathway, and the C - type lectin receptor signaling pathway.

In the Necroptosis signaling pathway, the mRNA expression levels of *Nlrp3* upstream genes *Ifnr* (2.2-fold) and *Jaks* (2.7-fold) were upregulated. In the NOD-like receptor signaling pathway, the mRNA expression levels of *Nlrp3* upstream genes *P2rx7*(5.6-fold),*Ip3r* (2.0-fold), and *Oas* (2.2-fold) were increased. In the C-type lectin receptor signaling pathway, the mRNA expression levels of *Nlrp3* upstream genes *Syk* (2.4-fold) and *Ip3r* (2.0-fold) were upregulated, while the mRNA expression levels of downstream genes *Nfat* and *Il-6* were downregulated by 2.0-fold.

Notably, in the NOD-like receptor signaling pathway, upon recognition of pathogen-associated molecular patterns (PAMPs) or damage-associated molecular patterns (DAMPs) by pattern recognition receptors (PRRs), certain stimuli (such as particulate matter deposition or lysosomal rupture) induce lysosomal damage, leading to the release of cathepsin B/L from lysosomes into the cytoplasm. The released cathepsin B/L directly cleaves NLRP3 or activates it via the reactive oxygen species (ROS) pathway. Oligomerized NLRP3 recruits the adaptor protein ASC (apoptosis-associated speck-like protein containing a CARD) through its PYD domain.

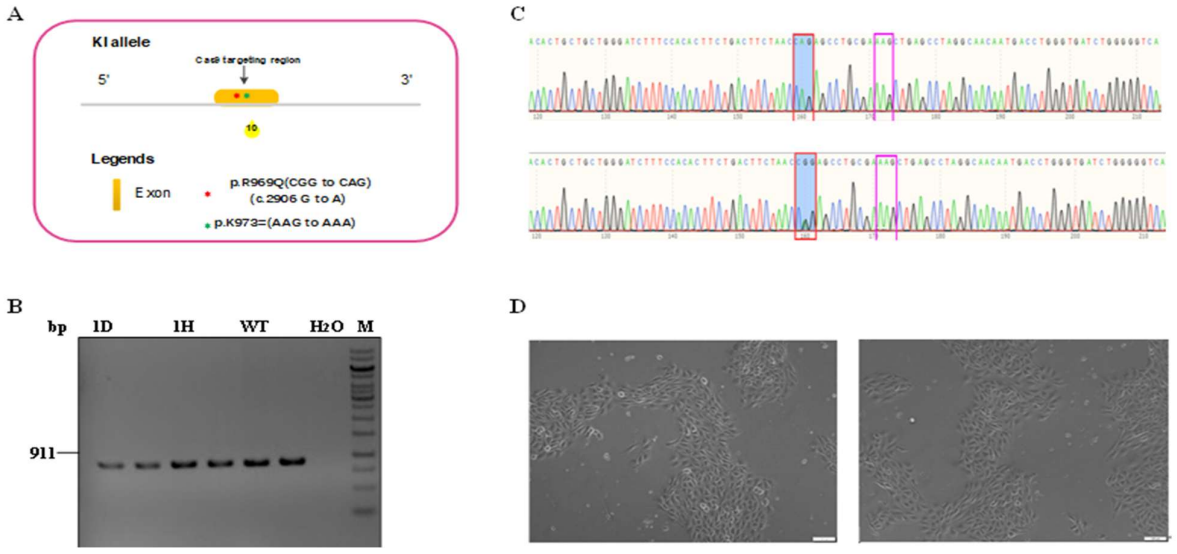

Fig.3: The point mutation of the 3D4/21 NLRP3 (p.R969Q) gene was constructed by CRISPR-Cas9 gene editing technology. (A) The process of constructing point mutations in the 3D4/21 NLRP3 (p.R969Q) gene. (B) Agarose gel electrophoresis of cells before and after point mutation of *NLRP3* (p.R969Q) gene (1D refer to PAM^{Q}, 1H refer to PAM^{R}, WT refer to wild-type cells). (C) Sequencing maps of the NLRP3 protein gene in PAM^{Q} (upper) and PAM^{R} (lower). (D)The status of cell clones (100^{x}, left is PAM^{Q}, right is PAM^{R}).

ASC undergoes prion-like polymerization to form large signaling complexes termed "ASC specks," which expose their CARD domains. Caspase-1 (CASP1) is then recruited to the ASC specks via CARD-CARD interactions. Upon auto-cleavage and activation, Caspase-1 cleaves pro-IL-1β (expressed following Signal 1 induction) to promote IL-1β maturation (Fig.6I). In this pathway, compared with the PAM^R group, the mRNA expression levels of PYD, Casp1, and IL-1β showed no significant changes in the PAM^Q group. This suggests that under Mhp stimulation, the observed differences in NLRP3 and IL-1β expression levels between PAM^R and PAM^Q are consistent with the divergence in their phagocytic function.

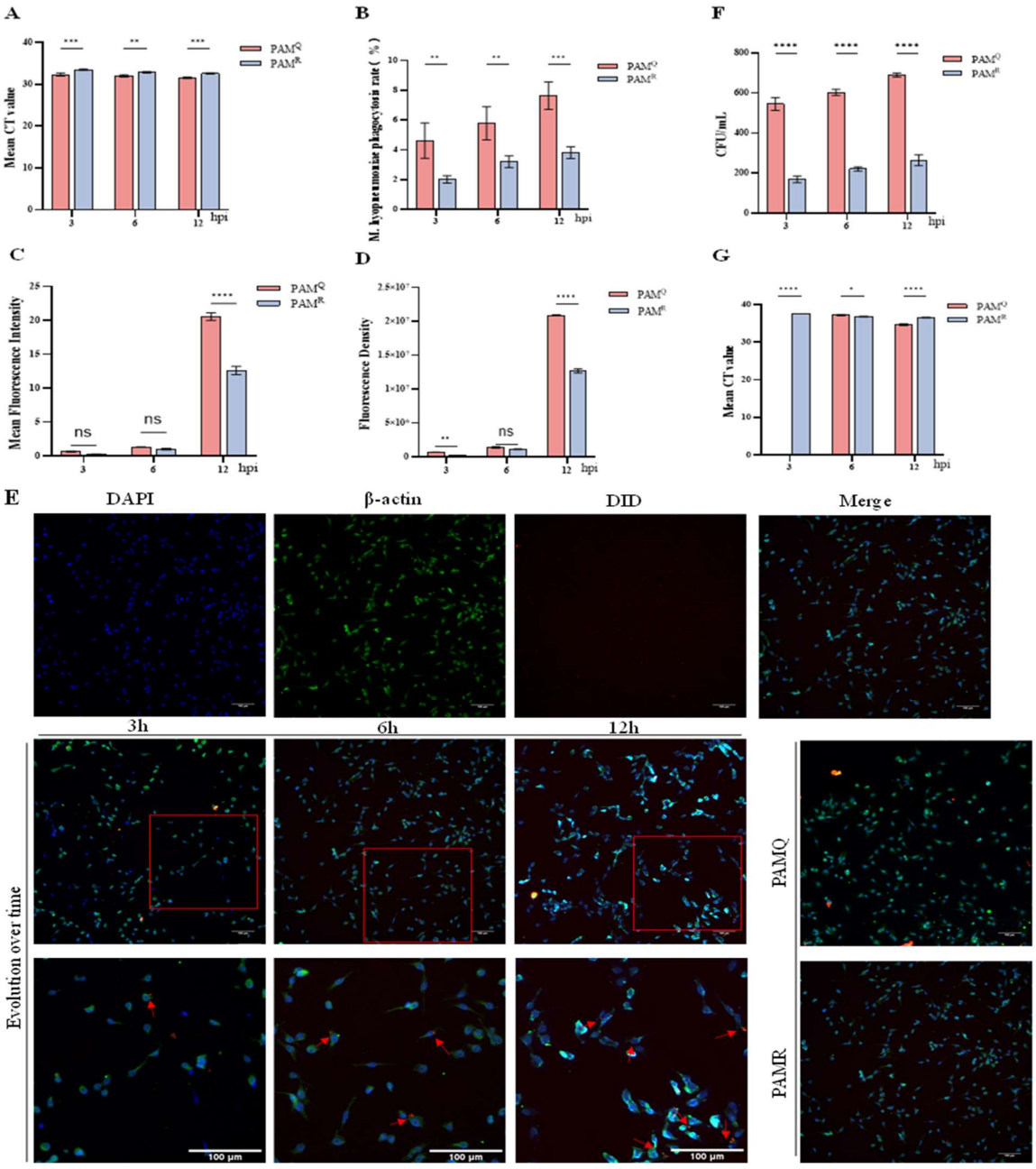

Fig.4: The *Nlrp3* c.2906A>G mutation regulates the efficiency of PAM in phagocytosing pathogenic microorganisms. (A) The phagocytic load of Mhp both PAM^Q and PAM^R were detected by qPCR, with Ct values from left to right being 32.32, 33.49, 31.98, 32.82, 31.57 and 32.57. (B)Difference in the efficiency in phagocytosing Mhp both PAM^Q and PAM^R, with phagocytic rates from left to right being 4.62, 2.01, 5.78, 3.20, 7.65, and 3.81%.(C)The average fluorescence intensities at 3, 6 and 12h were 0.67, 1.30, 20.57 for PAM^Q and 0.25, 1.04, 12.62 for PAM^R, respectively.(D)The fluorescence densities of PAM^Q and PAM^R at 3, 6 and 12h were 6.89×10^5, 1.38×10^6, 2.09×10^7 for PAM^Q and 2.57×10^5, 1.12×10^6, 1.27×10^7 for PAM^R, respectively. (E) Mhp was labeled with the DID fluorescent dye (red, red arrows), the cytoplasm of PAMs was stained with β-actin antibody (green), and the nucleus of PAMs were counterstained with DAPI (blue). Over time, the phagocytic capacity of PAMs for Mhp increased, and PAM^Q exhibited significantly stronger phagocytic ability than PAM^R. (F)The phagocytic efficiency of *Streptococcus suis* both PAM^Q and PAM^R were quantified separately by CFU assay, with values from left to right being 545, 169, 603, 221, 690 and 265CFU/mL. (G)The efficiency of PRRSV phagocytosed both PAM^Q and PAM^R were calculated separately based on the Ct values from qPCR, with Ct values from left to right being 0.00, 37.58, 37.19, 36.80, 34.64 and 36.56. Scale bar:100μm. Data are presented as the mean± SD (n=3 biological replicates). Statistical significance: ***P<0.0001, ***P <0.001, **P<0.01, *P<0.05 and ns, non-significant.

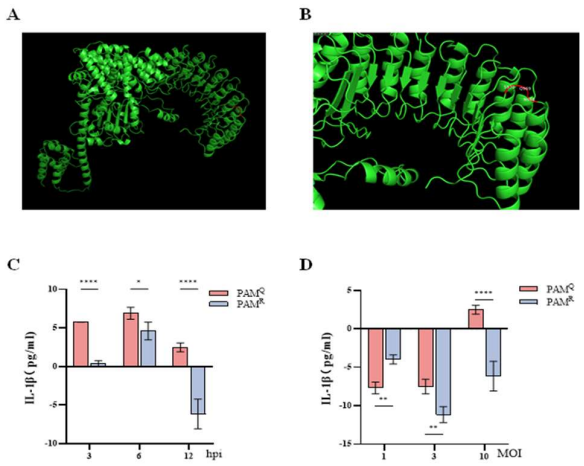

Fig.5: Prediction of NLRP3 protein structure and IL-1β secretion in PAM supernatants following Mhp stimulation. (A)The structure of NLRP3 protein was predicted through alphafold-3 simulation. (B)The mutation site is located in the loop region of the LRR domain (red line) of the NLRP3 protein. (C)At 3, 6 and 12 h post-stimulation, ELISA was used to detect the differences in IL-1β secretion between Mhp-challenged (treatment) and unstimulated (control) groups in PAM^Q and PAM^R cell supernatants. The calculated differences from left to right were 5.77, 0.38, 6.92, 4.62, 2.50 and −6.15 pg/mL, respectively. (D) IL-1β secretion differences between Mhp-stimulated (treatment) and unstimulated (control) groups in PAM^Q and PAM^R cell supernatants were measured by ELISA after 12 h of Mhp challenge at MOIs of 1, 3, and 10, with the values from left to right being −7.690, −3.977, −7.500, −11.15, 2.500, and −6.153 pg/mL, respectively.. Data are presented as the mean ± SD (n=3 biological replicates). Statistical significance: ****P<0.0001, ***P<0.001, **P<0.01, *P<0.05.

DISCUSSION

As one of the four famous indigenous pig breeds in China, Ningxiang pigs originated from Ningxiang County, Hunan Province, with thousands of years of breeding history (Li *et al*., 2021). Through long-term cultivation, Ningxiang pigs have developed tender and juicy meat with a unique flavor (Gong *et al*., 2021). As an important livestock resource in China, Ningxiang pigs were approved as a national geographical indication agricultural product by the Ministry of Agriculture in 2010 (Jiang *et al*., 2018). However, the breeding scale of Ningxiang pigs remains relatively small, primarily due to the high breeding costs that hinder their popularization. Their higher susceptibility to Mhp reduces growth rates, further increasing breeding costs. In this study, we established a direct link between the breed-specific susceptibility of Ningxiang pigs and a key genetic polymorphism in NLRP3, a critical innate immune regulator.

We initially observed that Ningxiang pigs exhibited a higher Mhp infection rate and more severe pulmonary histopathological damage compared to DLY pigs. These phenotypic differences were closely associated with a significant reduction in the phagocytic function of PAMs. This marked phenotypic divergence prompted further investigation into the underlying cellular and molecular mechanisms. Subsequent research revealed that all Ningxiang pigs carried the G allele (p.R969), whereas the majority of DLY pigs possessed the A allele (p.Q969). Site-directed mutagenesis to convert the G allele to the A allele in PAMs resulted in a significant increase (1.8- to 3.8-fold) in phagocytic efficiency against Mhp, definitively identifying the *Nlrp3*-2906G allele as the cause of impaired microbial clearance. This mutation significantly enhanced the phagocytic capacity of PAMs against both Mhp and *Streptococcus suis*. However, it exerted a time-dependent biphasic regulation on PRRSV clearance: suppressing viral phagocytosis at early stages while enhancing viral clearance at later stages. This indicates that the NLRP3 p.R969Q polymorphism shapes specific immune response patterns by differentially regulating bacterial and viral clearance mechanisms. The fundamental reason for the differential regulation of bacterial (Mhp/*Streptococcus suis*) and viral (PRRSV) phagocytic clearance by PAMs carrying this mutation lies in intrinsic differences in pathogen recognition mechanisms, invasion pathways, and immune signaling cascades. Notably, the phagocytic efficiency of Ningxiang pig-derived PAMs (p.R969) was weaker than that of DLY pig-derived PAMs (p.Q969), suggesting that the functional role of this locus may be complexly influenced by genetic background and requires further mechanistic clarification.

Activation and assembly of the NLRP3 inflammasome (Xu *et al*., 2021) lead to the formation of active IL-1β, which mediates inflammation (Xia *et al*., 2023). IL-1β plays a critical role in mediating inflammatory responses. To elucidate the molecular pathways downstream of this genetic variant, we conducted transcriptomic analysis. Transcriptome sequencing demonstrated that the p.Q969 (A allele) mutation significantly upregulated *Nlrp3* mRNA expression. Furthermore, although *Il-1β* mRNA levels showed no significant change, ELISA measurements revealed a substantial increase (1.5- to 15.2-fold) in IL-1β protein secretion in PAMs carrying the A allele. This clear disconnect between transcript and protein levels strongly suggests that the p.R969Q polymorphism enhances IL-1β production primarily at the post-transcriptional level, likely by promoting NLRP3 inflammasome assembly and subsequent Caspase-1-mediated proteolytic activation of pro-IL-1β. The absence of a dose-dependent IL-1β response to gradient Mhp stimulation further implies potential regulation by signal saturation or negative feedback mechanisms.

Upon receiving upstream signals, oligomerization of the NACHT domain of NLRP3 induces PYD clustering, which triggers the recruitment and aggregation of ASC. ASC clustering subsequently initiates the recruitment of Caspase-1 and the assembly of the inflammasome complex, followed by autoproteolytic cleavage of Caspase-1, which processes pro-inflammatory cytokines such as IL-1β and IL-18 into their active forms (He *et al*., 2016; Santa Cruz Garcia *et al*., 2022). Bioinformatic structural predictions locate the 969th residue within the LRR domain of NLRP3, a region critical for protein-protein interactions and inflammasome assembly. We hypothesize that the p.R969Q substitution alters the three-dimensional conformation of the LRR domain (Petrovskiy *et al*., 2023), thereby potentially enhancing the oligomerization efficiency of NLRP3 or its interaction with adaptor proteins such as ASC. Consequently, NLRP3 p.R969Q may confer an immune advantage against bacterial infections by enhancing Caspase-1-mediated processing efficiency of pro-IL-1β, rather than by increasing gene transcription.

Transcriptomic sequencing data indicated significant upregulation of *Nlrp3* only at the mRNA level (3.9-fold). However, mRNA and protein levels show only a moderate correlation (Arad and Geiger, 2023) and cannot be directly equated with synchronous increases in protein levels or

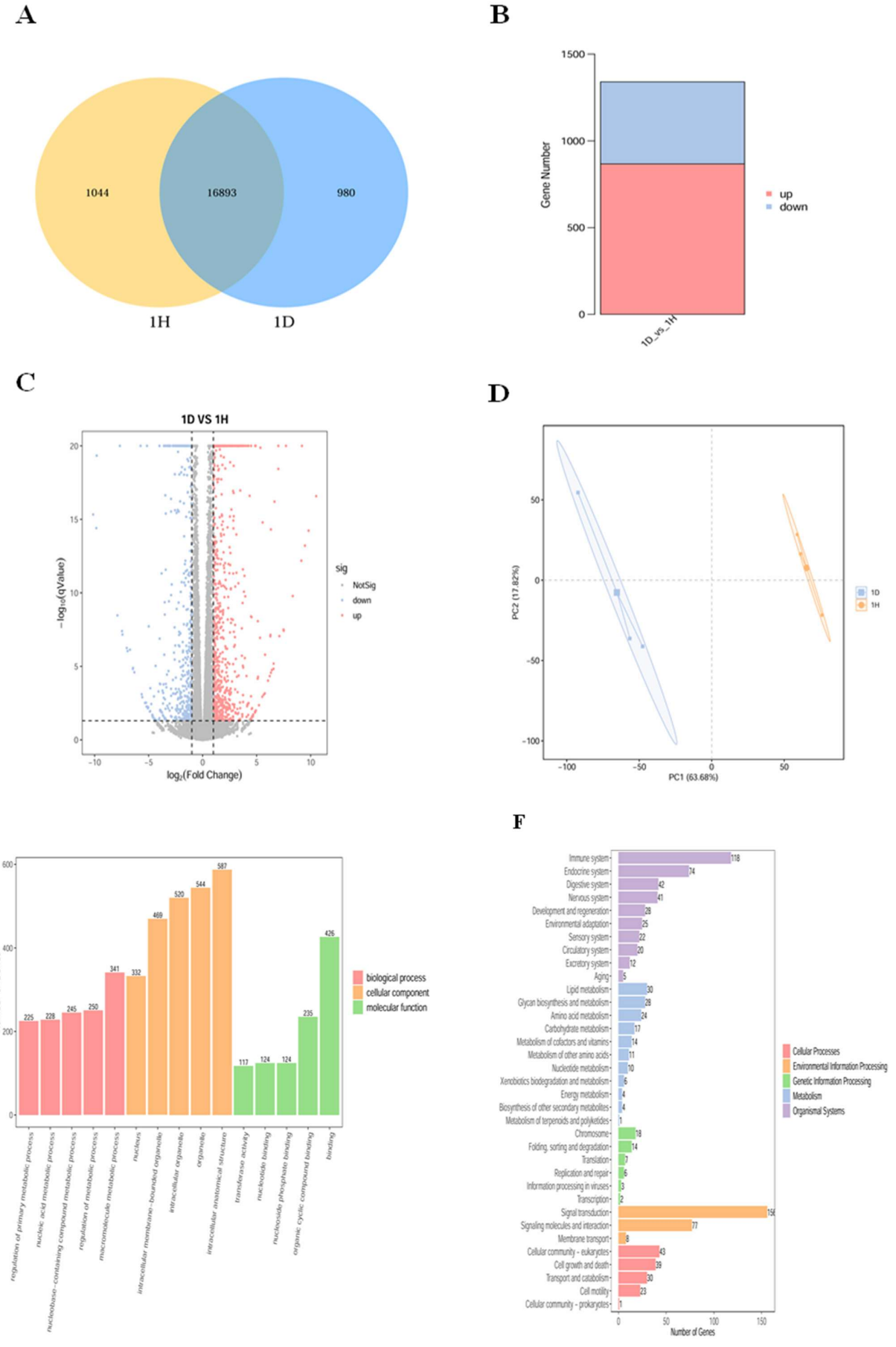
A
1044
16893
980
1H
1D
B
Gene Number
1500
1000
500
0
up
down
1D_vs_1H
C
1D VS 1H
−log10(qValue)
log2(Fold Change)
sig
NotSig
down
up
D
PC2 (17.82%)
PC1 (63.68%)
1D
1H
E
Number of Genes
biological process
cellular component
molecular function
regulation of primary metabolic process
nucleic acid metabolic process
nucleobase−containing compound metabolic process
regulation of metabolic process
macromolecule metabolic process
nucleus
intracellular membrane−bounded organelle
intracellular organelle
organelle
intracellular anatomical structure
transferase activity
nucleotide binding
nucleoside phosphate binding
organic cyclic compound binding
binding
F
Immune system
Endocrine system
Digestive system
Nervous system
Development and regeneration
Environmental adaptation
Sensory system
Circulatory system
Excretory system
Aging
Lipid metabolism
Glycan biosynthesis and metabolism
Amino acid metabolism
Carbohydrate metabolism
Metabolism of cofactors and vitamins
Metabolism of other amino acids
Nucleotide metabolism
Xenobiotics biodegradation and metabolism
Energy metabolism
Biosynthesis of other secondary metabolites
Metabolism of terpenoids and polyketides
Chromosome
Folding, sorting and degradation
Translation
Replication and repair
Information processing in viruses
Transcription
Signal transduction
Signaling molecules and interaction
Membrane transport
Cellular community - eukaryotes
Cell growth and death
Transport and catabolism
Cell motility
Cellular community - prokaryotes
Number of Genes
Cellular Processes
Environmental Information Processing
Genetic Information Processing
Metabolism
Organismal Systems

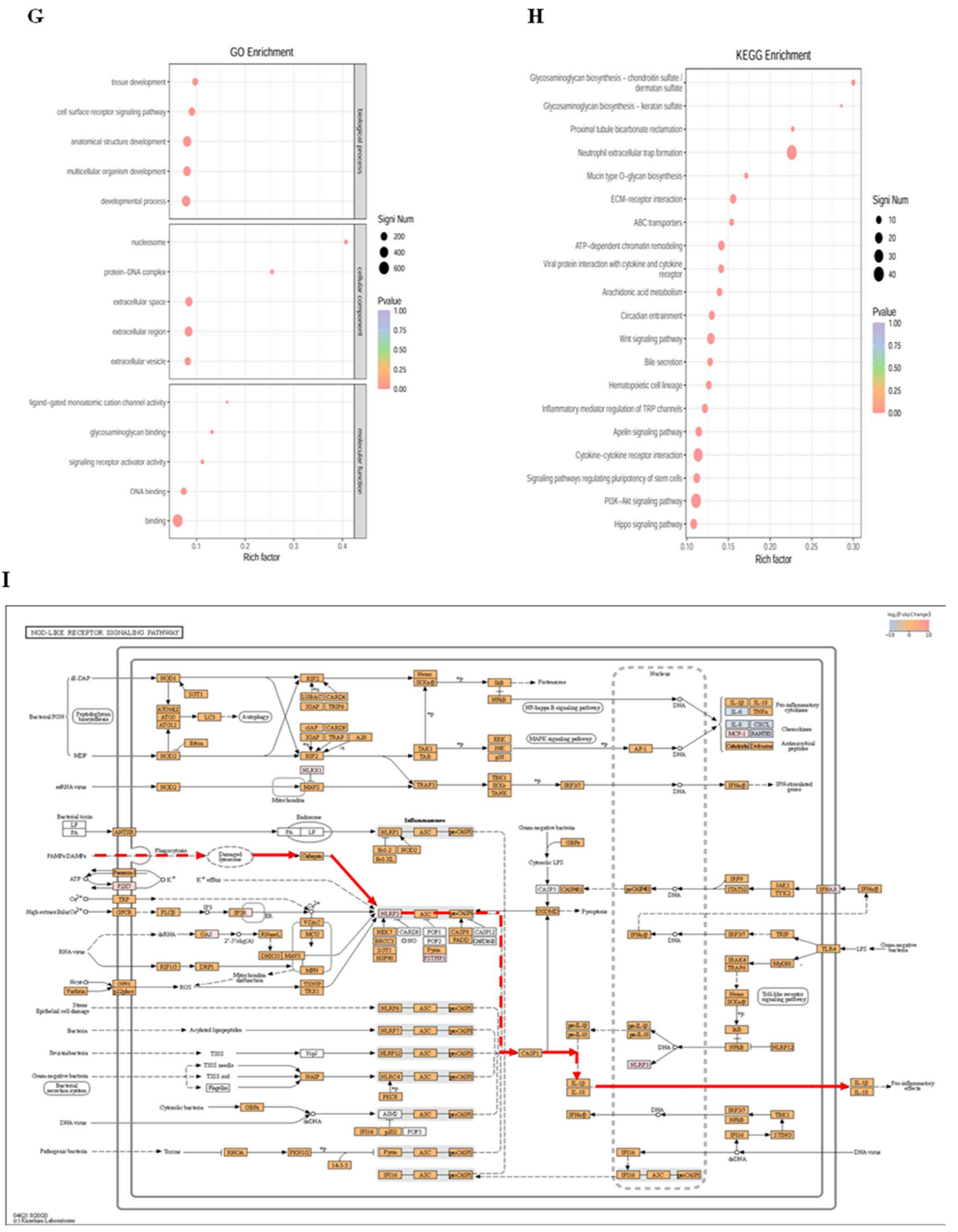

Fig.6: Transcriptome sequencing was performed after Mhp was co-incubated with PAM^{Q} and PAM^{R} respectively. (A) Venn diagram for visualising mutual and unique genes between PAM^{Q} (1D) and PAM^{R} (1H). (B) Statistical bar chart of expression differences**.** Horizontal Axis: Names of differential comparisons. Vertical Axis: Number of differentially expressed genes. Blue: Downregulated genes (867 genes). Red: Upregulated genes (473 genes). (C) Volcano Plot of Differentially Expressed Genes. The horizontal axis represents the log fold change (logFC) of genes across samples from different groups, while the vertical axis indicates the statistical significance of gene expression changes, where smaller q-values correspond to larger -log(q-values) and more significant differences. Each point in the plot represents a gene, with red denoting upregulated genes, blue indicating downregulated genes, and gray signifying genes with non-significant differences. (D) Principal component analysis (PCA) score plot. (E) Bar Chart of GO Annotations for Differentially Expressed Genes. The horizontal axis represents functional categories, with different colors denoting distinct classification branches. The vertical axis indicates the number of genes. (Sorted by q-value). (F)KEGG enrichment analysis of DEGs. (Sorted by q-value). (G) Significantly Enriched GO Terms Scatter Plot. (H) KEGG enrichment analysis of DEGs. (I) NOD-like receptor signaling pathway.

functional activity. Post-transcriptional regulation, differences in translation efficiency, and post-translational modifications and degradation are among the multiple factors that can contribute to discrepancies between mRNA and protein levels (Liu *et al*., 2016). Nonetheless, the significant upregulation of NLRP3 at the transcriptional level remains indicative of its involvement in the observed mechanisms.

Conclusions: The *Nlrp3*-2906G variant significantly impairs the phagocytic efficiency of PAMs against Mhp, thereby exacerbating Mhp susceptibility in Ningxiang pigs. Collectively, these findings unravel a novel genetic mechanism governing breed-specific susceptibility to Mhp. The results establish NLRP3 as a promising genetic marker for selective breeding programs focused on enhancing disease resistance in Chinese indigenous pig breeds.

Ethics approval and consent to participate: This was approved and consented to participate by the Biomedical Ethics Committee of Hunan Agricultural University, approval number 2024-140.

Data available: Raw data have been deposited to National Center for Biotechnology Information (NCBI) under the BioProject number PRJNA1358562.

Author's contribution: G.W.and M.L. designed experiments. L.Z. performed the majority of the experiments. Z.W., Z.Z. and G.Z. contributed to the isolation of the PAM from the DLY newborn piglets, IL-1β-ELISA, QPCR, Fluorescence tracing assay and GW score. J.Y. and S.Z contributed to the isolation of the PAM from the Ningxiang newborn piglets. X. H. contributed to the bioinformatics analysis. S.H., C.Y. and G.W. wrote and revised the manuscript. All authors discussed the results and contributed to the manuscript.

Declaration of interest: The authors declare that they have no conflict of interest.

Acknowledgments: The authors are grateful to Professor Jinhui Liu and Manager Qinghua Zeng for their clinical information and advice on Mhp in Ningxiang pigs, Professor Qigai He for providing the Mhp strains, Professor Wei Dong for providing the *Streptococcus suis* strains, Professor Meng Ge for providing the PRRSV strains, Chairman Shuchu Li and Professor Shiliu Yang assisted Hunan Liushahe Spotted Pig Ecological Animal Husbandry Co., Ltd. to provide Ningxiang newborn piglets, Manager Qiugen Zhao assisted Hunan New Wellful Co.,LTD to provide DLY newborn piglets. Xuwen Lu and Yaxin Chen sted in the collection of the lung samples of the slaughtered pigs.

Financial support statement: This study was supported by Projects funded by the National Natural Science Foundation of China (U23A20229),the key research and development project of Hunan Province (2023DK2004) and Hunan Agricultural University Scientific Research Project (No. 25SF053).

REFERENCES

Arad G and Geiger T, 2023. Functional impact of protein–RNA variation in clinical cancer analyses. Molecular and Cellular Proteomics 22:100587. https://doi.org/10.1016/j.mcpro.2023.100587

Arora P, Tewary S, Krishnamurthi S, *et al*., 2023. An experimental setup and segmentation method for CFU counting on agar plate for the assessment of drinking water. Journal of Microbiological Methods 214:106829. https://doi.org/10.1016/j.mimet.2023.106829

Chen S, Zhou Y, Chen Y, *et al*., 2018. fastp: an ultra-fast all-in-one FASTQ preprocessor. Bioinformatics 34:i884–i890. https://doi.org/10.1093/bioinformatics/bty560

Deeney AS, Maglennon GA, Chapat L, *et al*., 2019. Mycoplasma hyopneumoniae evades phagocytic uptake by porcine alveolar macrophages in vitro. Veterinary Research 50:51. https://doi.org/10.1186/s13567-019-0667-6

Duan Y, Zhang L, Angosto-Bazarra D, *et al*., 2020. RACK1 mediates NLRP3 inflammasome activation by promoting NLRP3 active conformation and inflammasome assembly. Cell Reports 33:108405. https://doi.org/10.1016/j.celrep.2020.108405

El-Sharkawy LY, Brough D and Freeman S, 2020. Inhibiting the NLRP3 inflammasome. Molecules 25:5533. https://doi.org/10.3390/molecules25235533

Fang XM, Zhao WM, Fu YF, *et al*., 2015. Difference in susceptibility to Mycoplasma pneumonia among various pig breeds and its molecular genetic basis. Scientia Agricultura Sinica 48:2839–2847. https://doi.org/10.3864/j.issn.0578-1752.2015.14.015

Ferreira MM, Mechler-Dreibi ML, Sonalio K, *et al*., 2021. Co-infections by Mycoplasma hyopneumoniae, Mycoplasma hyorhinis and Mycoplasma flocculare in macroscopic lesions of lung consolidation of pigs at slaughter. Veterinary Microbiology 258:109123. https://doi.org/10.1016/j.vetmic.2021.109123

Gilroy LC, Al-Kouatly HB and Mclaren RA, 2022. Statistical significance and clinical utility. American Journal of Obstetrics and Gynecology 227:372. https://doi.org/10.1016/j.ajog.2022.03.059

Gong Y, Zhang Y, Li B, *et al*., 2021. Insight into liver lncRNA and mRNA profiling at four developmental stages in Ningxiang pig. Biology 10:310. https://doi.org/10.3390/biology10040310

Guo S, Yang C, Diao B, *et al*., 2015. The NLRP3 inflammasome and IL-1β accelerate immunologically mediated pathology in experimental viral fulminant hepatitis. PLoS Pathogens 11:e1005155. https://doi.org/10.1371/journal.ppat.1005155

He Y, Hara H and Núñez G, 2016. Mechanism and regulation of NLRP3 inflammasome activation. Trends in Biochemical Sciences 41:1012–1021. https://doi.org/10.1016/j.tibs.2016.09.002

Janik E, Niemcewicz M, Ceremuga M, *et al*., 2020. Various aspects of a gene editing system—CRISPR–Cas9. International Journal of Molecular Sciences 21:9604. https://doi.org/10.3390/ijms21249604

Jiang Q, Li C, Yu Y, *et al*., 2018. Comparison of fatty acid profile of three adipose tissues in Ningxiang pigs. Animal Nutrition 4:256–259. https://doi.org/10.1016/j.aninu.2018.05.006

Kagan JC and Horng T, 2013. NLRP3 inflammasome activation: CD36 serves double duty. Nature Immunology 14:772–774. https://doi.org/10.1038/ni.2668

Keel BN, Nonneman DJ, Lindholm-Perry AK, *et al*., 2018. Porcine single nucleotide polymorphisms and their functional effect: an update. BMC Research Notes 11:860. https://doi.org/10.1186/s13104-018-3973-6

Kim D, Langmead B and Salzberg SL, 2015. HISAT: a fast spliced aligner with low memory requirements. Nature Methods 12:357–360. https://doi.org/10.1038/nmeth.3317

Lai J, He J and Ding H, 2023. Advances in innate immune responses induced by Mycoplasma hyopneumoniae infection. Chinese Journal of Biotechnology 39:4773–4783. https://doi.org/10.13345/j.cjb.230504

Li B, Yang J, He J, *et al*., 2021. Characterization of the whole transcriptome of spleens from Chinese indigenous breed Ningxiang pig reveals diverse coding and non-coding RNAs for immunity regulation. Genomics 113:2468–2482. https://doi.org/10.1016/j.ygeno.2021.05.025

Li L, Hu ZY, Kuang LS, *et al*., 2025. Exploring the dynamic changes of microorganisms and quality in cold-fresh Ningxiang pork during storage based on Illumina MiSeq sequencing and correlation analysis. Science and Technology of Food Industry 46:1–12. https://doi.org/10.13386/j.issn1002-0306.2025010024

Liu Y, Beyer A and Aebersold R, 2016. On the dependency of cellular protein levels on mRNA abundance. Cell 165:535–550. https://doi.org/10.1016/j.cell.2016.03.014

Maingi JW, Xiong QY, Wei YN, *et al*., 2014. Detection of respiratory pathogens Mycoplasma hyorhinis and Mycoplasma hyopneumoniae from clinically infected porcine using nested PCR in Jiangsu Province, China. Chinese Journal of Zoonoses 30:800–805. https://doi.org/10.3969/cjz.j.issn.1002-2694.2014.08.006

Mei X, Wang J, Zhang C, *et al*., 2023. Apigenin suppresses Mycoplasma-induced alveolar macrophages necroptosis via enhancing the methylation of TNF-α promoter by PPARγ-Uhrf1 axis. Phytomedicine 108:154504. https://doi.org/10.1016/j.phymed.2022.154504

Muneta Y, Uenishi H, Kikuma R, *et al*., 2003. Porcine TLR2 and TLR6: identification and their involvement in Mycoplasma hyopneumoniae infection. Journal of Interferon and Cytokine Research 23:583–590. https://doi.org/10.1089/107999003322485080

Ni L, Song C, Wu X, *et al*., 2019. RNA-seq transcriptome profiling of porcine lung from two pig breeds in response to Mycoplasma hyopneumoniae infection. PeerJ 7:e7900. https://doi.org/10.7717/peerj.7900

Pertea M, Pertea GM, Antonescu CM, *et al*., 2015. StringTie enables improved reconstruction of a transcriptome from RNA-seq reads. Nature Biotechnology 33:290–295. https://doi.org/10.1038/nbt.3122

Petrovskiy DV, Nikolsky KS, Rudnev VR, *et al*., 2023. Modeling side chains in the three-dimensional structure of proteins for post-translational modifications. International Journal of Molecular Sciences 24:13431. https://doi.org/10.3390/ijms241713431

Santa Cruz Garcia AB, Schnur KP, Malik AB, *et al*., 2022. Gasdermin D pores are dynamically regulated by local phosphoinositide circuitry. Nature Communications 13:52. https://doi.org/10.1038/s41467-021-27692-9

Shao JQ, 2003. Drugs and vaccines for the prevention and control of swine mycoplasmal pneumonia. China Animal Health:21–23.

Shen S, Park JW, Lu Z, *et al*., 2014. rMATS: robust and flexible detection of differential alternative splicing from replicate RNA-seq data. Proceedings of the National Academy of Sciences 111:E5593–E5601. https://doi.org/10.1073/pnas.1419161111

Shinkai H, Terada K, Toki D, *et al*., 2018. Q969R polymorphism in NLRP3 is associated with immune responses to vaccination against bacterial infections in pigs. Animal Science Journal 89:1043–1050. https://doi.org/10.1111/asj.13020

Sousa KRS, Dantas W de MF, de Oliveira LL, *et al*., 2024. Effect of vaccination against Mycoplasma hyopneumoniae on divergent pig genetic groups. Research in Veterinary Science 180:105417. https://doi.org/10.1016/j.rvsc.2024.105417

Subramanian A, Tamayo P, Mootha VK, *et al*., 2005. Gene set enrichment analysis: a knowledge-based approach for interpreting genome-wide expression profiles. Proceedings of the National Academy of Sciences 102:15545–15550. https://doi.org/10.1073/pnas.0506580102

Suzuki K, Shinkai H, Yoshioka G, *et al*., 2022. Polymorphisms in pattern recognition receptor genes are associated with respiratory disease severity in pig farms. Animals 12:3163. https://doi.org/10.3390/ani12223163

Tohno M, Shinkai H, Toki D, *et al*., 2016. Identification of the Q969R gain-of-function polymorphism in the gene encoding porcine NLRP3 and its distribution in pigs of Asian and European origin. Immunogenetics 68:693–701. https://doi.org/10.1007/s00251-016-0917-y

Wang GP, 2015. Study on the differentially expressed gene profiles of porcine alveolar macrophages induced by Mycoplasma pneumoniae. Doctoral dissertation. Hunan Agricultural University.

Wang G, Li J and Liu Y, 2024. Integrated analysis of differential gene expression profiles in porcine alveolar macrophages induced by Mycoplasma hyopneumoniae strain 232. Polish Journal of Veterinary Sciences:419–430. https://doi.org/10.24425/pjvs.2024.151735

Wang L, Wang S and Li W, 2012. RSeQC: quality control of RNA-seq experiments. Bioinformatics 28:2184–2185. https://doi.org/10.1093/bioinformatics/bts356

Wen Y, Chen Z, Tian Y, *et al*., 2022. Incomplete autophagy promotes the proliferation of Mycoplasma hyopneumoniae through the JNK and Akt pathways in porcine alveolar macrophages. Veterinary Research 53:62. https://doi.org/10.1186/s13567-022-01074-5

Xia J, Jiang S, Dong S, *et al*., 2023. The role of post-translational modifications in regulation of NLRP3 inflammasome activation. International Journal of Molecular Sciences 24:6126. https://doi.org/10.3390/ijms24076126

Xu M, Zheng J, Hu S, *et al*., 2021. Expression and immunogenicity study of a novel mhp183 gene fragment of Mycoplasma hyopneumoniae. Polish Journal of Veterinary Sciences 24:553–561. https://doi.org/10.24425/pjvs.2021.139980

Yin J, Li Y, Tian Y, *et al*., 2023. Obese Ningxiang pig-derived microbiota rewires carnitine metabolism to promote muscle fatty acid deposition in lean DLY pigs. The Innovation 4:100486. https://doi.org/10.1016/j.xinn.2023.100486

Yuan M, Guo X, Li N, *et al*., 2021. Silicon oxide-protected nickel nanoparticles as biomass-derived catalysts for urea electro-oxidation. Journal of Colloid and Interface Science 589:56–64. https://doi.org/10.1016/j.jcis.2020.12.100

Zhang Y, Liu B, Said A, *et al*., 2023. Regulatory functional role of NLRP3 inflammasome during Mycoplasma hyopneumoniae infection in swine. Journal of Animal Science 101:skad216. https://doi.org/10.1093/jas/skad216

Zhou YQ, 2021. Study on the role of Mycoplasma pneumoniae nuclease in escaping porcine alveolar macrophage extracellular traps. Master's thesis. Nanjing Agricultural University.

Zhou Y, Chen ZW, Duan QP, *et al*., 2025. Preliminary study on the mechanism of oxidative stress induced by Mycoplasma pneumoniae infection in porcine alveolar macrophages. Heilongjiang Animal Science and Veterinary Medicine:1–7. https://doi.org/10.13881/j.cnki.hljxmsy.2024.09.0024